Title page

Comparative proteomic analysis reveals the regulatory effects of H_2S on salt tolerance of mangrove plant *Kandelia obovata*

Authors: Yi-Ling Liu[1], Zhi-Jun Shen[1], Martin Simon[1], Huan Li[1], Dong-Na Ma[1], Xue-Yi Zhu[1] and Hai-Lei Zheng[1,2]

Institute or laboratory of origin:

[1] *Key Laboratory for Subtropical Wetland Ecosystem Research of MOE, College of the Environment and Ecology, Xiamen University, Xiamen, Fujian 361102, P. R. China*

[2] *Corresponding author (zhenghl@xmu.edu.cn)*

Corresponding author:
Hai-Lei Zheng, PhD, Professor
College of the Environment and Ecology, Xiamen University,
Xiamen, Fujian 361102, P.R. China
Tel: +86 592 218 1005
Fax: +86 592 218 5889
E-mail: zhenghl@xmu.edu.cn

Abstract: As a dominant mangrove species, *Kandelia obovata* is distributed in an intertidal marsh with an active H_2S release. Whether H_2S participates in the salt tolerance of mangrove plant is still ambiguous although increasing evidence have demonstrated that H_2S functions in plant responses to multiple abiotic stresses. In this study, as an H_2S donor, NaHS was used to investigate the regulatory mechanism of H_2S on salt tolerance of *K. obovata* seedlings using a combined physiological and proteomic analysis. The results showed that the reduction in photosynthesis (Pn) caused by 400 mM NaCl was recovered by the addition of NaHS (200 μM). Furthermore, the application of H_2S enhanced the quantum efficiency of PSII and the membrane lipid stability, implying that H_2S is beneficial to the survival of *K. obovata* seedlings under high salinity.

We further identified 37 differentially expressed proteins by proteomic approaches under salinity and NaHS treatment. Among them, the proteins related to photosynthesis, primary metabolism, stress response and hormone biosynthesis were primarily enriched. The physiological and proteomic results highlighted that exogenous H_2S up-regulated photosynthesis and energy metabolism to help *K. obovata* to cope with high salinity. Specifically, H_2S increased photosynthetic electron transfer, chlorophyll biosynthesis and carbon fixation in *K. obovata* leaves under salt stress. Furthermore, the abundances of other proteins related to metabolic pathway, such as antioxidation (APX, CSD2, PDX1), protein synthesis (HSP, Cpn 20), nitrogen metabolism (GS2, GS1:1), glycolysis (PGK, TPI), AsA-GSH cycle were increased by H_2S under high salinity. These findings provide new insights into the roles of H_2S in the adaptations of mangrove plant *K. obovata* to high salinity environment.

Keywords: *Kandelia obovata*, mangrove, hydrogen sulfide, salt tolerance, comparative proteome

Introduction

Mangroves is a complex and unique ecosystem that distributes along tropical and subtropical coastal tidal zone (Parida and Jha 2010). Mangroves are facultative halophytes and potential stress adaptors due to their special morphological, anatomical, physiological, and biochemical features (Parida and Jha 2010). Different mangrove species have different salinity preferences and achieve optimal growth at different salinity levels. Jayatissa et al. (2008) reported that there is an optimal growth for *Sonneratia caseolaris* with the lowest salt tolerance at 3-5 ppt salinity, and for *Avicennia marina* with the highest salt tolerance at 25-27 ppt salinity. As a dominant species of mangrove plants, *Kandelia obovata* can distribute in areas with salinities up to 27.58 ppt seawater level (Yang et al. 2013). The salinity between 5 and 15 ppt is suitable for indoor-cultured *K. obovata* growth, while salinity up to 20 ppt inhibits photosynthesis and growth of *K. obovata* (Li et al. 2008).

The tidal inundation, which originates from coastal waters, influences the sediment salinity and pore-water sulfide concentration (Watson et al. 2016). The soil salinities and porewater sulfide concentrations are further enhanced with high inundation (Luo et al. 2019). Hydrogen sulfide (H_2S) is the dominant sulfide-containing gas emitted from the intertidal sediment. During anaerobic decomposition, sulfate reduction in sediment was triggering, and H_2S was consequent producing, which annual mean is 768 ± 240 $\mu g \cdot S \cdot m^{-2}$ d^{-1} (Ganguly et al. 2018). Mangrove plants affect the sulfide concentration and H_2S emission flux in sediments (Lyimo et al. 2002), and this research focused on whether H_2S influences the adaptation of mangrove plants to harsh environmental conditions such as high salinity.

As a huge body of previous studies, plants gain their tolerance to abiotic stress by actively synthesizing H_2S. Hou et al. (2011) reported that drought stress led to stomatal closure through the increase in the expression and activity of D/L-cysteine desulfhydrase (L/D-CD), a key enzyme of H_2S biosynthesis in leaves of *Vicia faba*. H_2S pretreatment significantly increased regrowth ability of tobacco suspension-cultured cells re-growth ability after heat stress by alleviating a reduction in cell viability (Li et al. 2012). Salinity can detrimentally impact plant biomass production, which is associated with the salinity-induced (Yarsi et al. 2017). Previous studies mostly examined the role of H_2S in the mitigation of oxidative stress in salt-stressed plants (Christou et al. 2013; Sun and Luo 2014; Yu et al. 2013). The

activities of superoxide dismutase (SOD), catalase (CAT), ascorbic acid peroxidase (APX), glutathione reductase (GR), glutathione peroxidase (GPX) and dehydroascorbate reductase (DHAR) were increased in salt-stressed cucumber seedlings by the addition of NaHS which is a widely used H_2S donor, while under the same experimental conditions, lipid peroxide and hydrogen peroxide (H_2O_2) levels decreased (Yu et al. 2013). The improved germination rate of salt-stressed cucumber seed by H_2S might due to the breakdown of starch by H_2S-mediated α- and β-amylase in the endosperm, which ultimately led to improved hypocotyl growth (Sun and Luo 2014). To salt-stressed strawberry, pre-treatment roots with H_2S have a distinct increase in stomatal conductance, photosynthesis and leaf water content (Christou et al. 2013). In salt-stressed rice, NaHS increased chlorophyll and the content of protein (Mostofa et al. 2015). However, in the study of Koch et al. (1990), H_2S negatively affected the anoxic production of energy and the energy-dependent N uptake in roots of freshwater marsh species *Spartina alterniflora*.

In most of the true mangroves, the adaptations of seedlings to tolerate saline conditions have been widely studied (Krishnamurthy et al. 2014). However, the role of H_2S in salinity tolerance improvement in mangroves is still mostly unknown. In this study, an appropriate concentration of NaHS, a donor of H_2S, had a positive effect on *K. obovata* under high salinity considering both physiological and proteomic aspects. The *K. obovata* seedling were exposed to 400 mM NaCl with or without 200 μM NaHS for 7 days, and proteomics-based methodology (2-DE accompanied by MALDI-TOF/TOFMS) was adopted to investigate the specific metabolic pathways, and regulatory mechanism of H_2S on salt tolerance of *K. obovata* seedlings.

Materials and methods

Plant growth and treatment

Mature propagules of *K. obovata* were collected from the mangrove forest in the National Nature Reserve for Mangroves in Zhangjiang River Estuary (23°55’ N, 117°26’ E), Yunxiao County, Fujian Province, PR China, where salinity levels range from 8% to 20%. Healthy propagules of similar size (20 cm in length) were selected and pre-cultivated in a plastic pot (dimension of 12 cm in diameter and 11 cm in depth) with clean sands. The pots were placed in a growth chamber with temperature of 25/30 ℃ (night

/day), relative humidity of 70%, a photoperiod of 8 h dark/16 h light with around 1,250 μmol m^{-2} s^{-1}. A 1/4 strength Hoagland's nutrient solution was used to cultivate the hypocotyls. The solutions were replaced every week.

The treatments of NaHS and NaCl were set up when the 3rd pair of leaves appeared for physiological assays. The healthy and uniform seedlings were randomly cultivated in three groups and each group had three replicates.

In the first group, plants were supplied with NaHS and NaCl for 7 days. Different concentrations of NaHS at 0, 50, 100, 200, 350 and 500 μM (The average of H_2S is 243.1±234.9 μM in pore water samples of mangrove forest sediment) (Pérez et al. 2018) were prepared in the 1/4 strength Hoagland's nutrient solution in the presence or absence of 400 mM NaCl. After 7-days treatment, photosynthesis, chlorophyll content and dry weight were measured to determine the optimal NaHS concentration that growth inhibition induced by NaCl.

The second group was supplied with 1/4 strength Hoagland's nutrient solution containing 400 mM NaCl in the presence of NaHS (200 μM), Na_2SO4 (200 μM), $NaHSO_3$ (200 μM), $NaHSO_4$ (200 μM) and CH_3COONa (200 μM), respectively. Leaves were harvested after 7 days treatments for chlorophyll and endogenous H_2S content measurement to distinguish the actual role of H_2S/HS^- from the other possible compounds derived from NaHS decomposition.

According to the results from above two experiments, the third group was supplied with 1/4 strength Hoagland's nutrient solution containing 400 mM NaCl (NaCl) and 400 mM NaCl + 200 μM NaHS (NaCl+H_2S), respectively. The same volume of 1/4 strength Hoagland's nutrient solution was used as the control (CK). After chlorophyll fluorescence measurements, the second pair of leaves from the apex of the growing shoots were harvested and frozen rapidly in liquid nitrogen and stored at -80 ℃ for a proteomic study and further biochemical analysis.

Measurements of leaf photosynthetic pigment, photosynthetic rate and chlorophyll fluorescence quenching

The contents of chlorophyll were measured based Lichtenthaler (1987) with little modifications. 80% (v/v) acetone was used to extract chlorophyll, the content was estimated according to the absorbances at 470, 646 and 663 nm.

Net photosynthetic rate (Pn) of fully expanded leaves, as well as transpiration (Tr), stomatal conductance (Gs), and internal CO_2 concentration (Ci) were determined using a portable photosynthesis system (Li-6400, Li-Cor, Lincoln, NE, USA). Those measurements were carried out in the morning from 9:00 to 11:30. Recovery coefficient of Pn was calculated according to the following equation: Pn^{NaCl}/Pn^{CK}. Here, Pn^{NaCl} and Pn^{CK} stand for the leaf photosynthetic rate measured at NaCl and CK treatment.

We applied a fluorometer for measuring chlorophyll fluorescence (Li-6400, Li-Cor, Lincoln, NE, USA). Fv/Fm was calculated using $(F_m - F_0)/F_m$, where minimum (dark) fluorescence (F_0) was obtained by applying to measure light pulses at low frequency (0.03 μmol m^{-2} s^{-1} for 1 s). The maximum fluorescence (F_m) was determined by applying a saturating light pulse (6000 μmol m^{-2} s^{-1} for 0.8 s) to a dark-adapted sample (Neves et al. 2019).

Determination of dry weight and the content of endogenous H_2S

Endogenous H_2S content was determined according to Zhang et al (2008), and the method of Chen et al. (2014) was employed to determine the dry weight.

Measurements of oxidative stress and antioxidant system activity

The H_2O_2 content was measured according to Hung and Kao (2004). Lipid peroxidation in terms of malondialdehyde (MDA) content was measured according to Yan et al (2010).

For the relative electrolyte leakage (REL) measurement, fresh leaves (0.2 g) were cut, added to deionized water (20 mL) and degassed for 10 min at room temperature. Using an electrical conductivity meter (DDS-11A), the initial reading of conductivity (E1) was recorded. Then, the solution containing plant materials was incubated at 100 ℃ for 15 min. The final reading of conductivity (E2) of the solution was recorded after cooling. Besides, the reading of conductivity for deionized water (E0) was measured. Finally, the REL was estimated based on the following equation: REL (%) = (E1 - E0)/(E2 - E0) × 100%.

Superoxide dismutase (SOD) activity was determined according to the method described by Beauchamp and Fridovich (1971). Ascorbate peroxidase (APX) activity was estimated according to Chen and Asada (1989).

Total content of glutathione (GSH) was measured by a GSH kit (JBI, Nanjing, China). Leaves (0.3 g) were ground with 0.3 mL H_3PO_3 (25%) and 0.9 mL NaH_2PO_4-EDTA buffer (0.1 M, pH 8.0). The homogenates were separated at 10,000 *g* at 4℃ for 20 min. The supernatant was used for GSH content measurement (Devi and Prasad 1998). The absorbance at 420 nm was measured according to the manufacturer's instruction.

Protein extraction from *K. obovata* leaves and 2-DE PAGE and image/data analysis

Proteins were extracted by a phenol extraction procedure, followed by methanolic ammonium acetate precipitation, according to the method described by Delaplace et al. (2006). We rehydrated 17 cm immobilized pH 4-7 gradient strips (BioRad, CA, USA) with 340 μL rehydration buffer (contain 1 mg protein sample) in the tray for overnight. Ettan IPGphor3 system (GE Healthcare Amersham Bioscience, Little Chalfont, UK) was used to isoelectric focusing, following the condition described by Shen et al. (2018). In 12.5% acrylamide gels, we observed the gel electrophoresis. Each experiment was repeated three times.

We stained SDS-PAGE gels with Coomassie Brilliant Blue R-250 and scanned by Uniscan M3600 (China) at 600 dpi. Gels were analyzed by PDQuest software (Version 8.0, Bio-Rad) (Hu et al. 2014). Afterward, those proteins which compared to the control gels by over 2.0-fold changes were selected for the next experiment.

In-gel digestion, identification and classification of differentially expressed proteins

We excised the differentially expressed proteins (DEPs) with more than 2.0-fold change from 2-DE gels (Shen et al. 2018). Gel slices were incubated with 25 mM NH_4HCO_3 and acetonitrile for at least four times until the color of CBB was removed. Trypsin/Lys-C Mix (Promega, sequencing grade) was used to digest the proteins. Trifluoroacetic acid (0.5-1%) was added to terminate digestion. The supernatant was

collected at 12,000 × g for 10 minutes. MALDI-TOF-TOF mass spectrometer was used to analyze the supernatant for mass spectrometry identification (Applied Biosystems, Massachusetts, USA), according to Hu et al. (2014). The search parameters were set as follows: database NCBInr (release date: 2018.12.01); taxonomy viridiplantae (green plants); peptide mass ranged from 10 to 130 kDa; the coverage of protein sequence must reach a minimum of 10%; proteins with scores higher than 60 ($P < 0.05$); results with Confidence Interval % (C.I.%) value higher than 95% were considered to be an identifications.

The functions of the identified proteins were determined in http://www.uniprot.org/uniprot, and then the proteins were divided into five groups according to their biological functions in the plant. The subcellular localization of identified proteins was obtained by WoLF PSORT prediction tool (http://wolfpsort.hgc.jp/), as well as from previously published papers when possible.

The Search Tool of the Retrieval of Interaction Genes/Proteins (STRING) database was used to predict the protein-protein interactions (PPIs) (Szklarczyk et al. 2015) and Cytoscape to visualize significant protein-protein associations in the PPI network. The combined score of >0.4 was selected as the cut-off value. Then, module analysis was carried out by Molecular Complex Detection (MCODE) plugin to illuminate the biological significance of gene modules that respond to NaCl and/or NaHS treatment in *K.obovata* leaves (Bader and Hogue 2003). Subsequently, BiNGO tool was used to visualize the level of enriched GO terms.

Quantitative real-time PCR analysis

For the total RNA extraction, the frozen *K. obovata* leaves (0.1g) were ground in liquid nitrogen and extracted by using a Total RNA Kit (TaKaRa, Dalian, China). We observed the RNA quality and integrity by ultraviolet spectrophotometer (Cary 50, Varian, USA) and agarose gel electrophoresis. The RNA was used to synthesized cDNAs with M-MLV reverse transcriptase First-Strand cDNA synthesis kit (TaKaRa, Dalian, China), and the cDNA mixture was used as templates for subsequent PCRs. The primers used for real-time PCR were shown in Supplementary Table S1. A 10 μL real-time PCR mixture contained 2 μL primers, 2 μL cDNA, and 6 μL SYBR Green (Sangon, Shanghai, China). Five independent biological replicates were used to performed gene expression. The relative gene expression was calculated by the

$2^{-\Delta\Delta CT}$ method and actin was used as an internal control (Livak and Schmittgen 2001). The Bio-Rad iQ5 Multicolor Real-Time PCR Detection System (Bio-Rad, Hercules, CA) was used to run qRT-PCR.

Statistical analysis

Two-tailed Student's *t*-test ($P < 0.05$) was used for statistical analysis. Pearson's correlation among the amendment's characteristics was evaluated using SPSS Statistics for Windows (Version 22.0, IBM Corp, Armonk, NY). The direct and indirect relationships among leaf drought weight, chlorophyll content, net photosynthetic rate, intercellular carbon dioxide, stomatal conductance and transpiration rate were evaluated through path analysis using edgeR package. The heatmap of the DEPs was drawn by using R software "heatmap package".

Results

Effects of H_2S and NaCl on growth and photosynthesis of *K. obovata* seedlings

As expected, exogenous NaHS treatments (varying from 50 to 350 μM) progressively alleviated the NaCl-induced decrease in inhibition on leaf photosynthesis of *K. obovata* seedlings. Meanwhile, a high concentration of NaHS (500 μM) exhibited no beneficial effects (Figure 1). A powerful relationship was found among observed parameters through two-tailed Pearson correlation and path analysis (Supplementary Tables S2). Most of the physiological indices were positively correlated with the net photosynthetic rate (Pn) except intercellular carbon dioxide (Ci). The Pn had negative but significant associations (-0.655*) with Ci and displayed significant interactions with leaf dry weight (DW), chlorophyll content (Chl), stomatal conductance (Gs) and transpiration rate (Tr). Among different concentration of NaHS, 200 μM was the most effective in relieving NaCl-induced adverse effects in *K.obovata* seedlings. The recovery rate of Pn at 200 μM is the highest compared with other concentrations (Supplementary Figure S1). We used 200 μM NaHS in the next experiments.

H_2S rather than other derivatives from NaHS alleviates NaCl-induced reduction in chlorophyll content

It should be noticed that the NaHS solution contains not only H_2S/HS^- but also other sulfur-containing components. The research results showed that, except NaHS, the above chemicals failed to rescue NaCl-induced reduction of chlorophyll content only except NaHS (Supplementary Figure S2A). Meanwhile, leaf endogenous H_2S content kept the high level at NaHS treatment but maintained a stable low level under the negative controls when compared with the experimental control group (Supplementary Figure S2B). HS^- and/or H_2S has an essential role in relieving the reduction in chlorophyll content in *K. obovata* seedlings under salt treatment, but not other sulfur-containing compounds or sodium-containing compounds (Na_2SO_4, $NaHSO_3$, $NaHSO_4$, CH_3COONa).

Effects of H_2S and NaCl on the characteristics of chlorophyll fluorescence

The F_v/F_m ratio reflects the potential quantum efficiency of photosystem II (PSII), widely used as a sensitive indicator of stress-induced damage to the photosynthetic apparatus (Maxwell and Johnson 2000). After 7-days treatment with NaCl, *K. obovata* seedlings' leaves were used to measure the chlorophyll fluorescence. The results showed that NaCl treatment significantly decreased the ratio of F_v/F_m by 27.18% compared to the control. However, when exogenous H_2S was applied to NaCl-treated seedlings, the F_v/F_m was increased by 16.8% (Supplementary Figure S3).

Effects of H_2S and NaCl on oxidative stress and activity of the antioxidant system

Salinity was damaged to cytomembranes by increasing ROS. The content of H_2O_2 was analyzed to evaluate the effect of H_2S on the oxidative burst of NaCl-treated *K. obovata* seedlings. When exogenous H_2S was applied to NaCl-treated leaves, the content of H_2O_2 decreased from 5.36 $\mu mol \cdot g^{-1}$ to 4.79 $\mu mol \cdot g^{-1}$ (Figure 2A). Leaf REL and the content of MDA were measured to estimate the protective role of H_2S on the stability of membrane. Compared with NaCl treatment, the content of MDA was decreased from 0.71 $\mu mol \cdot g^{-1} \cdot FW$ to around 0.58 $\mu mol \cdot g^{-1}$ FW by exogenous H_2S addition (Figure 2B). Meanwhile, high salinity significantly increased REL of *K. obovata* leaves, being 2.0-fold higher than that of control. The exogenous H_2S significantly alleviated the NaCl-induced increase in REL (Figure 2C).

Additionally, the content of GSH significantly increased by around 4-fold after NaCl+H_2S treatment compared to the NaCl treatment (Figure 2D). Plant cells have evolved the antioxidant enzymatic system,

such as SOD and APX, to cope with stress-induced ROS generation. When exogenous H_2S was applied to NaCl-treated seedlings, APX activity increased by 6.1 U g^{-1} min^{-1} (Figure 2E), while the activity of SOD increased by about 315.3 U g^{-1} min^{-1} (Figure 2F) in comparison with the NaCl treatment.

Identification and classification of DEPs

The 2-DE proteomic approach was employed to analyze the protein expression profile to investigate the mechanism of H_2S-mediated salt tolerance of *K. obovata*. Three biological replicates were performed with similar results. According to the image analysis by PDQuest software, approximately 450 protein spots were reproducibly resolved on each gel. A total of 37 spots with significant changes (higher than 2.0-fold, $P < 0.05$) were identified as DEPs (Figure 3A).

We provide 37 DEPs information in Table 1. A comprehensive overview of expression patterns of 37 identified proteins is shown in Figure 4A. They were divided into five functional categories, including carbohydrate and energy metabolism (29.73%), photosynthesis (18.92%), stress response proteins and cell structure (18.92%), amino acid and protein metabolism (16.22%), hormone biosynthesis and transcription factor (10.81%) by the biological function, which is in the UniProt database (Figure 4B). Comparing with NaCl vs CK group, there were more up-regulated DEPs in NaCl+H_2S vs CK group. These up-regulated DEPs were mostly divided into carbohydrate and energy metabolism, and stress response proteins (Figure 4B).

STRING interaction networks among DEPs

To predict protein-protein interaction (PPI) networks by STRING database, alignment of the amino acid sequence to find the corresponding homologous proteins from *Arabidopsis thaliana*. The PPI network visualized by Cytoscape is shown in Supplementary Figure S4. The PPI network of DEPs is composed of 27 nodes and 129 edges. A total of 2 modules were identified in the PPI network, which includes 9 and 8 proteins, respectively (Figure 5, Supplementary Table S3). Module A has 9 nodes and 32 interactions. The key node in module A is GS2. Module B has 8 nodes and 22 interactions. The key node in module B is RBCL.

An acyclic graph was constructed and directed using the BiNGO tool to depict the visual interactions of functions based on the enrichment levels of the GO terms. The present study identified eight significantly enriched GO terms in biological processes, and especially in terms of response to response to abiotic stimulus, response to stress, and generation of precursor metabolites and energy (Supplementary Figure S5).

Comparisons of expression patterns between protein and transcript of selected DEPs

To further verify the results of the proteome, we randomly selected 6 DEPs to further analyze their transcriptional expressions under different treatments by using quantitative real-time PCR. Particularly, the consistency between protein level and mRNA level of the following proteins was compared: transcription factor bHLH145 (spot 13), superoxide dismutase 4 (SOD, spot 18), heat-shock protein (HSP, spot 19), oxygen-evolving enhancer protein 1 (OEE1, spot 14), abscisic acid stress ripening protein (Asr, spot 31) and glutamine synthetase 1;1 (GS1;1, spot 33). The detailed list of the corresponding primer pairs and the detailed PCR procedures used for the real-time PCR are summarized in the Supplemental Table S1. As shown in Figure 6, all selected genes showed a similar pattern with their corresponding protein.

Discussion

H_2S but not other NaHS derivatives contributes to chlorophyll content recovery decreased by NaCl treatment

NaHS, which in solution dissociates to Na^+ and HS^- that associates with H^+ producing H_2S, is widely used to examine biological effects of H_2S (Hosoki et al. 1997). To discriminate the effects of NaHS from other sulfur- and sodium-containing compounds, solutions of Na_2SO_4, $NaHSO_3$, $NaHSO_4$, and CH_3COONa were used instead of NaHS to ameliorate NaCl-induced seedling growth inhibition. In contrast to the results from NaHS, treatment with other compounds failed to induce endogenous H_2S accumulation and to alleviate the reduction in chlorophyll content caused by NaCl exposure (Supplementary Figure S2). Accordingly, this study provides evidence that NaHS-associated responses are H_2S-specific.

Exogenous H_2S alleviates growth and photosynthesis inhibition induced by NaCl in *K. obovata* seedlings

Parameters such as relatively low fresh and dry weight and reduced photosynthesis are potential indicators of salinity stress in plants (Yarsi et al. 2017). In this study, significant variations in studied physiological traits of *K. obovata* under different concentrations of NaHS with 400 mM NaCl were recorded. Low concentration of H_2S (50-350 μM) increased the *K. obovata* leaf dry weight, chlorophyll content, and photosynthesis. In contrast, when the concentration of H_2S reached 500 μM, the above indices all decreased (Figure 1). These findings are in agreement with Chen et al. (2011), who reported a similar decline in the biomass and photosynthesis of *Spinacia oleracea* after treatment with a high concentration of NaHS.

The previous study indicated that H_2S could indirectly enhance photosynthesis reaching their maximal values, as well as the maximal photochemical efficiency of photosystem II (F_v/F_m) (Chen et al. 2011). In the present research, NaCl+H_2S treatment also increased F_v/F_m (Supplementary Figure S3). Additionally, the proteomics analyses revealed six proteins involved in the light reactions of photosynthesis, including electron transfer, light-harvesting, and light-induced oxidation of water. The level of ferredoxin-NADP reductase (FNR, spot 2), which catalyzes the removal of the electron from PSI to $NADP^+$, and otherwise NADPH is oxidized to produce reducing power via ferredoxin (Fd) (Mulo and Medina 2017), recovered under NaCl+H_2S treatment. The O_2 evolving complex 33kD family protein (OEC spot 12) has been termed the chloroplast manganese-stabilizing protein due to its functions in assembly, stabilization and protection of the manganese cluster required for oxygen evolution in higher plants (Sugihara et al. 2000). The accumulation of OEC came back to control level under NaCl+H_2S treatment, which implied that H_2S maintained the photosynthetic electron transport activity during *K. obovata* exposure to high salt stress. Besides, NaCl-induced down-regulation of photosynthetic electron transfer C (PETC, spot 10) which is the important subunit of Cytb_6f complex and participates the linear electron transport (Sanda et al. 2011), was alleviated by the addition of H_2S. Nevertheless, plastocyanin (PC, spot 1) was up-regulated under NaCl, which is consistent with the study on *K. candel* under high salinity did by Wang et al. (2015). On another hand, the abundances of PC remained unchanged under combined NaCl+NaHS treatment. The results of proteomics analyses are in agreement with physiological measurements which showed that treatment with NaHS alleviated the NaCl-caused inhibition of photosynthesis.

Photosynthetic carbon assimilation is driven by ribulose-1,5-bisphosphate (RuBP) carboxylase (Rubisco). Ribulose-1,5-bisphosphate carboxylase large subunit (RBCL, spot 8) was down-regulated by NaCl treatment and unchanged under NaCl+NaHS treatment. Noteworthy, ribulose activase small isoform precursor (RBCS, spot 36) showed a reverse trend, which is unchanged under NaCl treatment and down-regulated by NaCl+NaHS treatment. The capacity of photosynthesis is associated with the level of RBCL/RBCS ratio in rice leaves (Wang et al. 2009). The up-regulation of RCA and RBCL/RBCS ratio by NaHS addition under salt treatment in our study indicated that the alleviation of Rubisco inhibition inevitably lead to the improvement of photosynthesis.

Phosphoglycolate phosphatase (PGP, spot 25), which is involved in photorespiration and required for giving carbon from 2-phosphoglycolate back into metabolism (Bauwe et al. 2012). The photosynthetic electron transport was more allocated to photorespiration with the decrease of the chlorophyll content (Bauwe et al. 2012). In this study, NaCl treatment strongly up-regulated PGP, which indicated allocation of photosynthetic electron transport to Calvin cycle was reduced (Wingler et al. 2000).

The photosynthetic electron transport chain converts light into chemical energy, supplying ATP and NADPH to drive the carbon dioxide reduction and fixation processes (Matuszyńska et al. 2019). ATP synthase CF1 epsilon subunit (atpC, spot 7) is involved in energy supply needed for carbon dioxide reduction and fixation processes. Compared with NaCl treatment, atpC were recovered under NaCl+H_2S treatment, implying the energy used for photosynthetic carbon assimilation was recovered with NaHS addition.

H_2S rescues the primary metabolism altered by NaCl

In this study, triosephosphate isomerase (TPI, spots 16), and phosphoglycerate kinase (PGK, spot 35) were found to be unchanged or down-regulated under high salinity. PGK plays a crucial role in catalyzing the ATP-dependent phosphorylation of phosphoglycerate in the Calvin cycle (Zhao et al. 2016). The two glycolytic enzymes were all positivity modulated by NaHS addition, suggesting much more energy was produced by glycolysis.

All levels of plant function are affected by nitrogen metabolism (Schultz et al. 1998). In higher plants, glutamine synthetase (GS2 and GS1:1, spot 32 and 33) is a crucial enzyme of primary ammonium assimilation and nitrogen metabolism (Lea and Miflin 2003). Glutamine synthetase participates in the synthesis of GSH through glutamate biosynthesis pathway; thus, the overexpression of glutamine synthetase leads to more GSH formation (Sarry et al. 2006; Semane et al. 2010). It is interesting to note that the accumulation of glutamine synthetase was positivity modulated by NaHS addition.

Heat-shock protein (HSP, spot 19) and 20 kDa chaperonin family protein (Cpn 20, spot 26), which involved in protein synthesis, were found positivity modulated by NaHS addition. As molecular chaperones, HSP and chaperonin family protein participate in protein transport, protein folding, and protein assembly processes (Omar et al. 2011). During abiotic stress, chaperonins help the plant to combat against increasing amount of incorrectly folded proteins (Omar et al. 2011).

Previous publications have reported that the TCA cycle provides essential precursors for amino acid biosynthesis and energy metabolism. ATP synthase subunit d (ATP5PD, spot 9) and ATP synthase beta subunit (ATP5F1B, spots 29) are located in the mitochondria. The ATP synthase is an important enzyme which catalyzes energy production by synthesizing ATP from ADP (Yasuda et al. 2001), providing energy to the TCA cycle. NaCl+H_2S treatment significantly up-regulated the accumulation of ATP5PD and ATP5F1B. In addition, nucleoside diphosphate kinase 1 (NDPK1, spot 30), a housekeeping enzyme that maintains the levels of CTP, GTP, and UTP in cells, was identified to be down-regulated under high salinity and significantly up-regulated by NaHS addition. A recent study showed that NDPK granted transgenic plants tolerance to multiple stresses, including salt and extreme temperatures (Dorion and Rivoal 2015).

Remarkably, H_2S rescued the primary metabolism altered by NaCl. In a previous study, Li et al. (2016) also reported that increment in energy metabolism by H_2S might be responsible for abiotic stress alleviation.

H_2S relieves oxidative stress induced by NaCl

Salt-induced disruption of the normal plant metabolism results in accumulation of harmful reactive oxygen species (ROS) (Hernandez and Almansa 2002). Excess ROS not only causes growth inhibition but also programmed cell death (PCD). The accumulation of H_2O_2, and consequent increase in MDA and REL are indicators of salt-induced oxidative damage to the membranes (Demiral and Turkan 2005). In the present study, NaHS pretreatment reduced the accumulation of H_2O_2, MDA, and REL under salt stress, which is in agreement with the previous study by Shi et al. (2013). In addition, Actin7 isoform 1 (Actin7, spot 23) is thought to aid in the stability of organelles membranes in plant cells and induces PCD with the stabilization of actin depolymerization (Geitmann and Nebenfuhr 2015, Thomas et al. 2006), was significantly up-regulated under NaCl+H_2S treatment. Meanwhile, plants trigger various enzymatic and non-enzymatic antioxidants to detoxify ROS and prevent cellular damage (Yin et al. 2019). In this study, compared with NaCl treatment, the activity of superoxide dismutase (SOD) and cytosolic ascorbate peroxidase (APX), and the content of GSH were found to be induced by application of H_2S (Figure 2). Ascorbate (AsA) and GSH play important roles in the AsA-GSH cycle (Suo et al. 2015). As an electron donor, APX reduces H_2O_2 into the water using AsA, and monodehydroascorbate can react with GSH to produce AsA and oxidized GSH catalyzed by DHAR (Suo et al. 2015). The increase in GSH content and the activity of APX indicate that H_2S promoted AsA-GSH cycle responsible for the removal of H_2O_2 under high salinity. In agreement, APX (spot 37) protein expression was found up-regulated under NaCl+H_2S treatment. Moreover, copper/zinc superoxide dismutase CSD2A-1 (CSD2, spot 17) was found up-regulated under NaCl+H_2S treatment, but SOD (spot 18) showed the opposite trend. We propose that CSD2 plays a critical role in a direct and rapid mechanism of ROS detoxification under high salinity. In short, based on the above results, it can infer that H_2S has a positive effect to protect the plant from the excess ROS.

Moreover, some abiotic stress-related proteins, such as cysteine proteinase (CP, spot 4), pyridoxine biosynthesis PDX1-like protein 3 (PDX1, spot11), and alcohol dehydrogenase (ADH, spots 20) also responded to high salinity and NaCl+H_2S treatment. An increase in the CP activity occurred just before the first senescence symptoms became visible in most plants (Buono et al. 2019). CP is involved in PCD and the balance between the levels of CP and phytocystatins is keeping in a certain state through the antagonistic activities of ABA and GAs (Prins et al. 2008, Szewińska et al. 2016). The accumulation of CP was significantly down-regulated by NaHS addition. PDX1 was identified as a cysteine synthase (Komatsu

et al. 2014), inducing cysteine biosynthesis as a protective measure against high ion concentrations, or synthesis of cystatin to inhibit PCD (Youssefian et al. 1993). We observed that PDX1 was significantly up-regulated under NaCl+H_2S treatment.

H_2S regulates hormone biosynthesis and transcription factor

Abscisic acid stress ripening protein (Asr, spot 31) is a downstream protein, which participates in ABA signaling pathways (Shkolnik and Bar-Zvi 2008). The bHLH served as negative feedback regulatory loop in ABA signaling in *Arabidopsis thaliana* (Zheng et al. 2019). In the present study, the up-regulated of Asr and bHLH145 under salt treatment and recovered under NaCl+H_2S treatment, which indicated the signal transduction of ABA was inhibited by the addition of NaHS. Furthermore, in the promoter regions of the genes encoding CP exists ABA-responsive elements (Szewińska et al. 2016). Besides, NaHS up-regulated the accumulation of bZIP (spot 27), which positively altered the adaptation of plants to adverse circumstances (Joo et al. 2013; Sen et al. 2017).

Protein-protein interaction networks analysis

The DEPs in the PPI network exhibited higher enrichment, indicating a higher degree of modularization; therefore, the DEPs were divided into two modules for investigating the interactions using Mode (Figure 5). In module A, CDSP, FLDH (NAD(P)-binding Rossmann-fold superfamily protein isoform 1, spot 24), FNR, GS2, OEE, PC, PETC, RBCS are enriched in response to stimulus. The key node in this module is GS2. In module B, six nodes (APX, Cpn20, TPI, PGK, Prx, SOD) are involved in response to abiotic stimulus and another two nodes (RBCL, ATP5F1B) are related to Calvin cycle. The two modules implied that response to abiotic stimulus influenced other biological process.

Conclusions

Physiological, and proteomic evidence in this study support beneficial role of H_2S on *K. obovata* exposed to high salinity: (1) H_2S increased carbon fixations and electron transfer, maintaining photosynthesis under high salinity; (2) H_2S stimulated glycolysis to generate precursor metabolites and energy, and protein synthesis; (3) H_2S increased enzymatic and non-enzymatic antioxidants to detoxify ROS and prevent cellular damage under high salinity; (4) H_2S effected the ABA signaling pathway, which

led to sustained plant adaptation to high salinity. As shown in Figure 7, we propose a working model to illustrate the detailed mechanism by which H_2S alleviates the NaCl-induced inhibition. In conclusion, these findings have important implications for understanding the functional role of H_2S in salt tolerance of *K. obovata*.

Acknowledgments

This study was jointly supported by the funds from the National Key Research and Development Program of China (2017YFC0506102), and the Natural Science Foundation of China (NSFC 31570586 and 31870581).

Reference

1. Bader GD, Hogue CW (2003) An automated method for finding molecular complexes in large protein interaction networks. BMC Bioinformatics 4(1):2.
2. Beauchamp C, Fridovich I (1971) Superoxide dismutase: improved assays and an assay applicable to acrylamide gels. Anal Biochem 44(1):276-287.
3. Buono RA, Hudecek R, Nowack MK (2019) Plant proteases during developmental programmed cell death. J Exp Bot 70(7):2097-2112.
4. Caruso G, Cavaliere C, Guarino C, Gubbiotti R, Foglia P, Lagana A (2008) Identification of changes in *Triticum durum* L. leaf proteome in response to salt stress by two-dimensional electrophoresis and MALDI-TOF mass spectrometry. Anal Bioanal Chem 391(1):381-390.
5. Chen GX, Asada K (1989) Ascorbate peroxidase in tea leaves: occurrence of two isozymes and the differences in their enzymatic and molecular properties. Plant Cell Physiol 30(7):987-998.
6. Chen J, Liu TW, Hu WJ, Simon M, Wang WH, Chen J, Liu X, Zheng HL (2014) Comparative proteomic analysis of differentially expressed proteins induced by hydrogen sulfide in *Spinacia oleracea* leaves. PLoS ONE 9(9):e105400.
7. Chen J, Wu FH, Wang WH, Zheng CJ, Lin GH, Dong XJ, He JX, Pei ZM, Zheng HL (2011) Hydrogen sulphide enhances photosynthesis through promoting chloroplast biogenesis, photosynthetic enzyme expression, and thiol redox modification in *Spinacia oleracea* seedlings. J Exp Bot

433 62(13):4481-4493.
434 8. Chichkova S, Arellano J, Vance CP, Hernandez G (2001) Transgenic tobacco plants that overexpress
435 alfalfa NADH-glutamate synthase have higher carbon and nitrogen content. J Exp Bot
436 52(364):2079-2087.
437 9. Christou A, Manganaris GA, Papadopoulos I, Fotopoulos V (2013) Hydrogen sulfide induces
438 systemic tolerance to salinity and non-ionic osmotic stress in strawberry plants through modification
439 of reactive species biosynthesis and transcriptional regulation of multiple defence pathways. J Exp Bot
440 64(7):1953-1966.
441 10. Delaplace P, van der Wal F, Dierick JF, Cordewener JHG, Fauconnier ML, du Jardin P, America
442 AHR (2006) Potato tuber proteomics: Comparison of two complementary extraction methods
443 designed for 2-DE of acidic proteins. Proteomics 6(24):6494-6497.
444 11. Demiral T, Turkan I (2005) Comparative lipid peroxidation, antioxidant defense systems and proline
445 content in roots of two *rice* cultivars differing in salt tolerance. Environ Exp Bot 53(3):247-257.
446 12. Devi SR, Prasad MNV (1998) Copper toxicity in *Ceratophyllum demersum* L. (Coontail), a free
447 floating macrophyte: response of antioxidant enzymes and antioxidants. Plant Sci 138(2):157-165.
448 13. Dorion S, Rivoal J (2015) Clues to the functions of plant NDPK isoforms. N-S Arch Pharmacol
449 388(2):119-132.
450 14. Ganguly D, Ray R, Majumdar N, Chowdhury C, Jana TK (2018) Biogenic hydrogen sulphide
451 emissions and non-sea sulfate aerosols over the Indian Sundarban mangrove forest. J Atmos Chem
452 75(3):319-333.
453 15. Geitmann A, Nebenfuhr A (2015) Navigating the plant cell: intracellular transport logistics in the
454 green kingdom. Mol Biol Cell 26(19):3373-3378.
455 16. Hernandez JA, Almansa MS (2002) Short-term effects of salt stress on antioxidant systems and leaf
456 water relations of pea leaves. Physiol Plant 115(2):251-257.
457 17. Hosoki R, Matsuki N and Kimura H (1997) The possible role of hydrogen sulfide as an endogenous
458 smooth muscle relaxant in synergy with nitric oxide. Biochem Biophys Res Co 237(3):527-531.
459 18. Hou ZH, Liu J, Hou LX, et al. (2011) H_2S may function downstream of H_2O_2 in jasmonic
460 acid-induced stomatal closure in *Vicia faba*. Chin Bull Bot 46(4):396-406.

19. Hu WJ, Chen J, Liu TW, et al. (2014) Proteome and calcium-related gene expression in *Pinus massoniana* needles in response to acid rain under different calcium levels. Plant Soil 380(1-2):285-303.

20. Hung KT, Kao CH (2004) Hydrogen peroxide is necessary for abscisic acid-induced senescence of rice leaves. J Plant Physiol 161(12):1347-1357.

21. Jayatissa LP, Wickramasinghe W, Dahdouh-Guebas F, et al. (2008) Interspecific variations in responses of mangrove seedlings to two contrasting salinities. Int Rev Hydrobiol 93(6):700-710.

22. Jiang J, Gai Z, Wang Y, et al. (2018) Comprehensive proteome analyses of lysine acetylation in tea leaves by sensing nitrogen nutrition. BMC Genomics 19(1):840.

23. Joo J, Lee YH, Kim YK, et al. (2013) Abiotic stress responsive rice *ASR1* and *ASR3* exhibit different tissue-dependent sugar and hormone-sensitivities. Mol Cells 35(5):421-435.

24. Koch MS, Mendelssohn IA, Mckee KL (1990) Mechanism for the hydrogen sulfide-induced growth limitation in wetland macrophytes. Limnol Oceanogr 35(2):399-408.

25. Komatsu S, Kamal AH, Hossain Z (2014) Wheat proteomics: proteome modulation and abiotic stress acclimation. Front Plant Sci 5:684.

26. Krishnamurthy P, Tan XF, Lim TK, et al. (2014) Proteomic analysis of plasma membrane and tonoplast from the leaves of mangrove plant *Avicennia officinalis*. Proteomics 14(21-22):2545-2557.

27. Lea PJ, Miflin BJ (2003) Glutamate synthase and the synthesis of glutamate in plants. Plant Physiol Bioch 41(6-7): 555-564.

28. Lerslerwong L, Ketsa S, van Doorn WG (2009) Protein degradation and peptidase activity during petal senescence in *Dendrobium* cv. Khao Sanan. Postharvest Biol Tech 52(1):84-90.

29. Li D, Limwachiranon J, Li L, et al. (2016) Involvement of energy metabolism to chilling tolerance induced by hydrogen sulfide in cold-stored banana fruit. Food Chem 208:272-278.

30. Li N, Chen S, Zhou X, et al. (2008) Effect of NaCl on photosynthesis, salt accumulation and ion compartmentation in two mangrove species, *Kandelia candel* and *Bruguiera gymnorhiza*. Aquat Bot 88(4):303-310.

31. Li ZX, Liu C, Zhang Y, et al. (2019) The bHLH family member ZmPTF1 regulates drought tolerance in maize by promoting root development and ABA synthesis. J Exp Bot 70(19):5471-5486.

32. Li ZG, Gong M, Xie H, et al. (2012) Hydrogen sulfide donor sodium hydrosulfide-induced heat tolerance in tobacco (*Nicotiana tabacum* L) suspension cultured cells and involvement of Ca^{2+} and calmodulin. Plant Sci 185:185-189.

33. Lichtenthaler HK (1987) Chlorophylls and carotenoids: pigments of photosynthetic biomembranes. Method Enzymol 148: 350-382.

34. Livak KJ, Schmittgen TD (2001) Analysis of relative gene expression data using real-time quantitative PCR and the 2- ΔΔCT method. Methods 25(4):402-408.

35. Luo M, Huang JF, Zhu WF, et al. (2019) Impacts of increasing salinity and inundation on rates and pathways of organic carbon mineralization in tidal wetlands: a review. Hydrobiologia 827(1):31-49.

36. Lyimo TJ, Pol A, den Camp HJO (2002). Sulfate reduction and methanogenesis in sediments of Mtoni mangrove forest, Tanzania. Ambio 31(7):614-617.

37. Matuszyńska A, Saadat NP, Ebenhoeh O (2019) Balancing energy supply during photosynthesis-a theoretical perspective. Physiol Plant 166(1):392-402.

38. Maxwell K, Johnson GN (2000) Chlorophyll fluorescence-a practical guide. J Exp Bot 51(345):659-668.

39. MittlerR, Vanderauwera S, Gollery M, et al. (2004) Reactive oxygen gene network of plants. Trends Plant Sci 9(10):490-498.

40. Mostofa MG, Saegusa D, Fujita M, et al. (2015) Hydrogen sulfide regulates salt tolerance in rice by maintaining Na^+/K^+ balance, mineral homeostasis and oxidative metabolism under excessive salt stress. Front Plant Sci 6:1055

41. Mulo P, Medina M (2017) Interaction and electron transfer between ferredoxin-$NADP^+$ oxidoreductase and its partners: structural, functional, and physiological implications. Photosynth Res 134(3):265-280.

42. Neves LH, Santos RIN, dos Santos Teixeira GI, et al. (2019) Leaf gas exchange, photochemical responses and oxidative damages in assai (*Euterpe oleracea* Mart.) seedlings subjected to high temperature stress. Sci Hortic 257:108733.

43. Omar SA, Fu QT, Chen MS, et al. (2011) Identification and expression analysis of two small heat shock protein cDNAs from developing seeds of biodiesel feedstock plant *Jatropha curcas*. Plant Sci

181(6):632-637.

44. Oukarroum A, Bussotti F, Goltsev V, et al. (2015) Correlation between reactive oxygen species production and photochemistry of photosystems I and II in *Lemna gibba* L. plants under salt stress. Environ Exp Bot 109:80-88.

45. Parida AK, Jha B (2010) Salt tolerance mechanisms in mangroves: a review. Trees-Struct Funct 24(2):199-217.

46. Pérez A, Gutiérrez D, Saldarriaga M S, et al. (2018) Tidally driven sulfidic conditions in Peruvian mangrove sediments. Geo-Marine Letters 38(5): 457-465.

47. Prins A, Van Heerden PD, Olmos E, et al. (2008) Cysteine proteinases regulate chloroplast protein content and composition in tobacco leaves: a model for dynamic interactions with ribulose-1,5-bisphosphate carboxylase/oxygenase (Rubisco) vesicular bodies. J Exp Bot 59(7):1935-1950.

48. Sanda S, Yoshida K, Kuwano M, et al. (2011) Responses of the photosynthetic electron transport system to excess light energy caused by water deficit in wild watermelon. Physiol Plant 142(3):247-264.

49. Sarry JE, Kuhn L, Ducruix C, et al. (2006) The early responses of *Arabidopsis thaliana* cells to cadmium exposure explored by protein and metabolite profiling analyses. Proteomics 6(7):2180-2198.

50. Schultz CJ, Hsu M, Miesak B, et al. (1998) Arabidopsis mutants: Define an in *vivo* role for isoenzymes of aspartate aminotransferase in plant nitrogen assimilation. Genetics 149(2):491-499.

51. Semane B, Dupae J, Cuypers A, et al. (2010) Leaf proteome responses of *Arabidopsis thaliana* exposed to mild cadmium stress. J Plant Physiol 167(4):247-254.

52. Sen S, Chakraborty J, Ghosh P, et al. (2017) Chickpea WRKY70 regulates the expression of a homeodomain-leucine zipper (HD-Zip) I rranscription factor *CaHDZ12*, which confers abiotic stress tolerance in transgenic tobacco and chickpea. Plant Cell Physiol 58(11):1934-1952.

53. Shen ZJ, Chen J, Ghoto K, et al. (2018) Proteomic analysis on mangrove plant *Avicennia marina* leaves reveals nitric oxide enhances the salt tolerance by up-regulating photosynthetic and energy metabolic protein expression. Tree Physiol 38(11):1605-1622.

54. Shi H, Ye T, Chan Z (2013) Exogenous application of hydrogen sulfide donor sodium hydrosulfide

545 enhanced multiple abiotic stress tolerance in bermudagrass (*Cynodon dactylon* (L). Pers.). Plant
546 Physiol Bioch 71:226-234.
547 55. Shkolnik D, Bar-Zvi D (2008) Tomato ASR1 abrogates the response to abscisic acid and glucose in
548 *Arabidopsis* by competing with AB14 for DNA binding. Plant Biotechnol J 6(4):368-378.
549 56. Sugihara K, Hanagata N, Dubinsky Z, et al. (2000) Molecular characterization of cDNA encoding
550 oxygen evolving enhancer protein 1 increased by salt treatment in the mangrove *Bruguiera*
551 *gymnorrhiza*. Plant Cell Physiol 41(11):1279-1285.
552 57. Sun YD, Luo WR (2014) Effects of exogenous hydrogen sulphide on seed germination and seedling
553 growth of cucumber (*Cucumis sativus*) under sodium bicarbonate stress. Seed Sci Technol
554 42(2):126-131.
555 58. Suo JW, Zhao Q, Zhang ZX, et al. (2015) Cytological and proteomic analyses of osmunda
556 cinnamomea germinating spores reveal characteristics of fern spore germination and rhizoid tip
557 growth. Mol Cell Proteomics 14(9):2510-2534.
558 59. Szewińska J, Simińska J, Bielawski W (2016) The roles of cysteine proteases and phytocystatins in
559 development and germination of cereal seeds. J Plant Physiol 207: 10-21.
560 60. Szklarczyk D, Franceschini A, Wyder S, et al. (2015) STRING v10: protein-protein interaction
561 networks, integrated over the tree of life. Nucleic Acids Res 43(D1):D447-452.
562 61. Thomas SG, Huang SJ, Li ST, et al. (2006) Actin depolymerization is sufficient to induce
563 programmed cell death in self-incompatible pollen. J Cell Biol, 174(2):221-229.
564 62. Van Noort JM, Kraal B, Bosch L, et al. (1984) Cross-linking of tRNA at two different sites of the
565 elongation factor Tu. P Natl A Sci 81(13):3969-3972.
566 63. Wang D, Lu Q, Li XF, et al. (2009) Relationship between Rubisco activase isoform levels and
567 photosynthetic rate in different leaf positions of rice plant. Photosynthetica 47(4):621-629.
568 64. Wang L, Pan DZ, Li J, et al. (2015) Proteomic analysis of changes in the *Kandelia candel* chloroplast
569 proteins reveals pathways associated with salt tolerance. Plant Sci 231:159-172.
570 65. Watson EB, Szura K, Wig and C, et al. (2016) Sea level rise, drought and the decline of *Spartina*
571 *patens* in New England marshes. Biol Conserv 196:173-181.
572 66. Whitney SM, Houtz RL, Alonso H (2011) Advancing our understanding and capacity to engineer

nature's CO_2-sequestering enzyme, Rubisco. Plant Physiol 155(1):27-35.

67. Wingler A, Lea PJ, Quick WP, et al. (2000) Photorespiration: metabolic pathways and their role in stress protection. Philos T R Soc B 355(1402):1517-1529.

68. Yan K, Chen W, Zhang G, et al. (2010) Elevated CO_2 ameliorated oxidative stress induced by elevated O_3 in *Quercus mongolica*. Acta Physiol Plant 32(2):375-385.

69. Yang SC, Shih SS, Hwang GW, et al.(2013) The salinity gradient influences on the inundation tolerance thresholds of mangrove forests. Ecol Eng 51:59-65

70. Yarsi G, Sivaci A, Dasgan HY, et al. (2017) Effects of salinity stress on chlorophyll and carotenoid contents and stomata size of grafted and ungrafted galia C8 melon cultivar. Pak J Bot 49(2):421-426.

71. Yasuda R, Noji H, Yoshida M, et al. (2001) Resolution of distinct rotational substeps by submillisecond kinetic analysis of F-1-ATPase. Nature 410(6831):898-904.

72. Yin ZP, Zhang H, Zhao Q, et al. (2019) Physiological and comparative proteomic analyses of saline-alkali $NaHCO_3$-responses in leaves of halophyte *Puccinellia tenuiflora*. Plant Soil 437(1-2):137-158.

73. Youssefian S, Nakamura M, Sano H (1993) Tobacco plants transformed with the O-acetylserine (thiol) lyase gene of wheat are resistant to toxic levels of hydrogen sulphide gas. Plant J 4(5):759-769.

74. Yu L, Zhang C, Shang H, et al. (2013) Exogenous hydrogen sulfide enhanced antioxidant capacity, amylase activities and salt tolerance of cucumber hypocotyls and radicles. J Integr Agr 12(3):445-456.

75. Zhang H, Hu LY, Hu KD, et al (2008) Hydrogen sulfide promotes wheat seed germination and alleviates oxidative damage against copper stress. J Integr Plant Biol 50(12):1518-1529.

76. Zhao Q, Suo JW, Chen SX, et al. (2016) Na_2CO_3-responsive mechanisms in halophyte *Puccinellia tenuiflora* roots revealed by physiological and proteomic analyses. Sci Rep 6:32717.

77. Zheng K, Wang Y, Wang S (2019) The non-DNA binding bHLH transcription factor Paclobutrazol Resistances are involved in the regulation of ABA and salt responses in Arabidopsis. Plant Physiol Bioch 139:239-245.

598 **Figure captions**

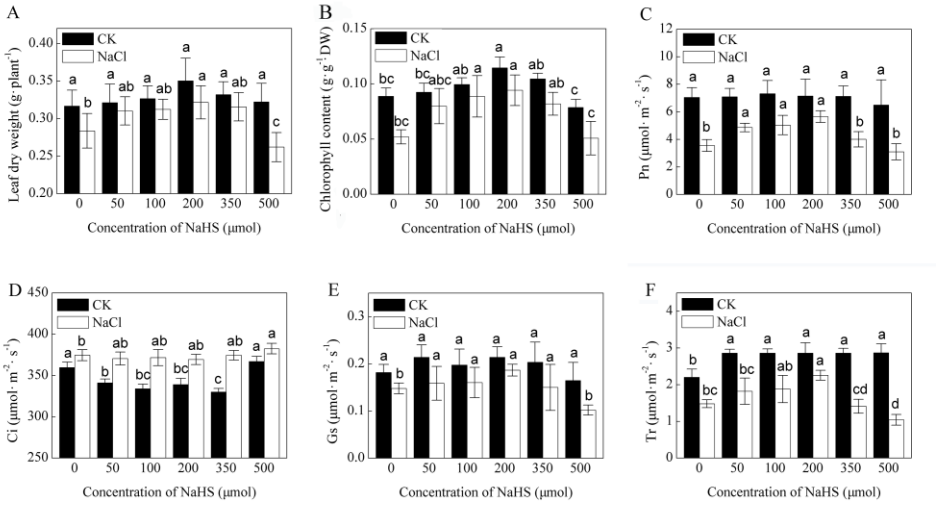

599

600 **Figure 1.** Effects of various concentrations of NaHS on leaf photosynthetic characteristics of *K. obovata*
601 seedlings treated by high salinity. (A) leaf dry weight, (B) total chlorophyll contents, (C) net photosynthetic
602 rate (Pn), (D) intercellular CO_2 concentration (Ci), (E) stomatal conductance (Gs) and (F) transpiration rate
603 (Tr). Seedlings were treated with different concentrations of NaHS (0, 50, 100, 200, 350 and 500 μM)
604 together with 400 mM NaCl for 7 days. Values are means ± SE of three independent experiments with at
605 least three replicates for each. Bars with different letters are significantly different at $P < 0.05$ according to
606 Duncan's multiple range test.

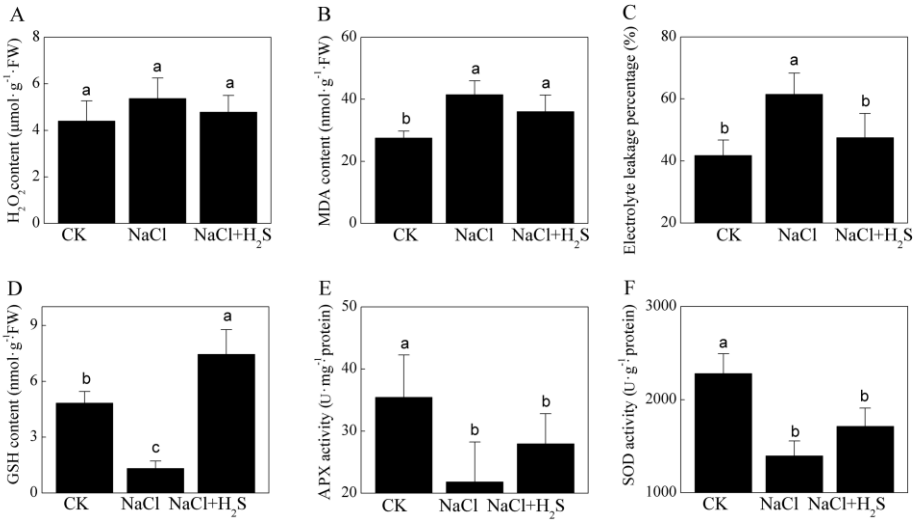

607

Figure 2. Effects of NaHS on oxidative stress and antioxidant system activity of the leaves of *K. obovata* seedlings treated by high salinity. (A) H_2O_2 content, (B) malondialdehyde (MDA) content, (C) electrolyte leakage percentage, (D) glutathione (GSH) content, (E) ascorbate acid peroxidase (APX) activity and (F) superoxide dismutase (SOD) activity. CK stands for the control treated only by 1/4 strength Hoagland's nutrient solution. NaCl stands for 400 mM NaCl treatment. NaCl+H_2S stands for 400 mM NaCl + 200 μM NaHS treatment. Error bars are SE (n =3). The columns labeled with different letters are significantly different at $P < 0.05$.

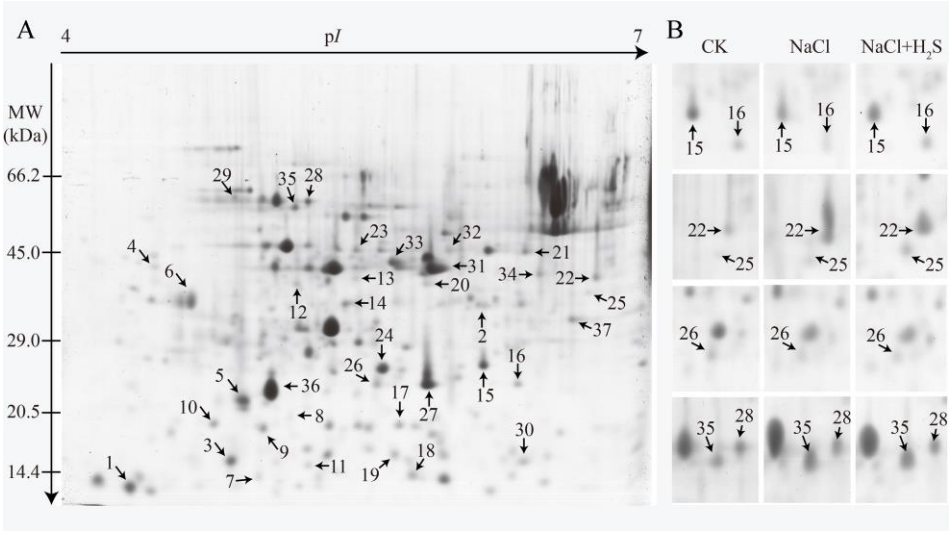

Figure 3. 2-DE analysis of proteins extracted from the leaves of *K. obovata* seedlings exposed to NaCl and combined NaCl and NaHS treatments. The numbers assigned to the protein spots correspond to those listed in Table 1. (A) Representative CBB-R250 stained 2D gel of total proteins extracted from *K. obovata* leaves under the control condition. Proteins (1.5 mg) were loaded onto the pH 4-7 gradient IPG strip for the first-dimensional isoelectric focusing (IEF) and then separated in the second dimension on a 15% SDS-PAGE gel. The isoelectric point (p*I*) and molecular weight (MW) in kilodaltons are indicated on the top and left of the gel. Arrows indicate 37 spots with at least 2.0-fold changes ($P < 0.05$) that were analyzed by MALDI-TOF/TOF MS. (B) The enlarged windows of the representative protein spots with different expression under NaCl and NaCl+H_2S treatments. NaCl stands for 400 mM NaCl treatment, NaCl+H_2S stands for 400 mM NaCl + 200 μM NaHS treatment, and CK stands for the control treated only by 1/4 strength Hoagland solution.

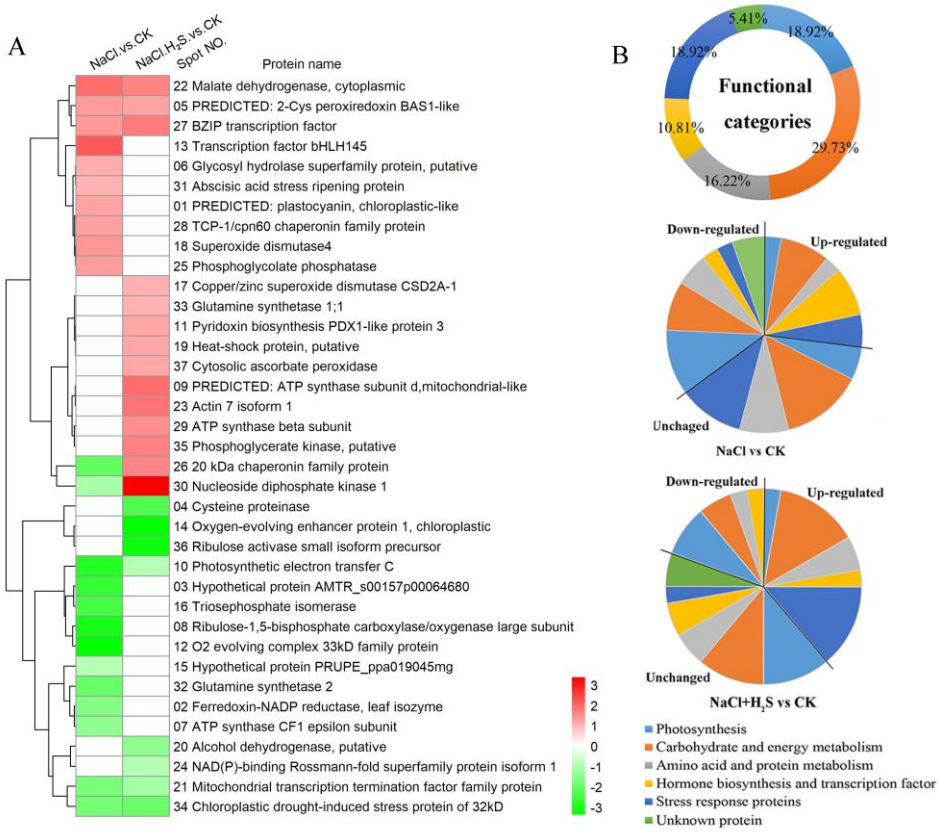

627

628 **Figure 4.** (A) Functional classification and hierarchical clustering analysis, (B) Functional categories for
629 the 37 differentially expressed proteins in *K. obovata* seedling leaves under NaCl and NaCl+H_2S treatments.
630 The rows represent the individual protein. The protein cluster is on the left side, and the treatment cluster is
631 on the top. The up- or down-regulated proteins are indicated in red or green and white represent no change.
632 The intensity of the color increases with increasing expression differences, as shown in the bar at the
633 bottom of the figure.

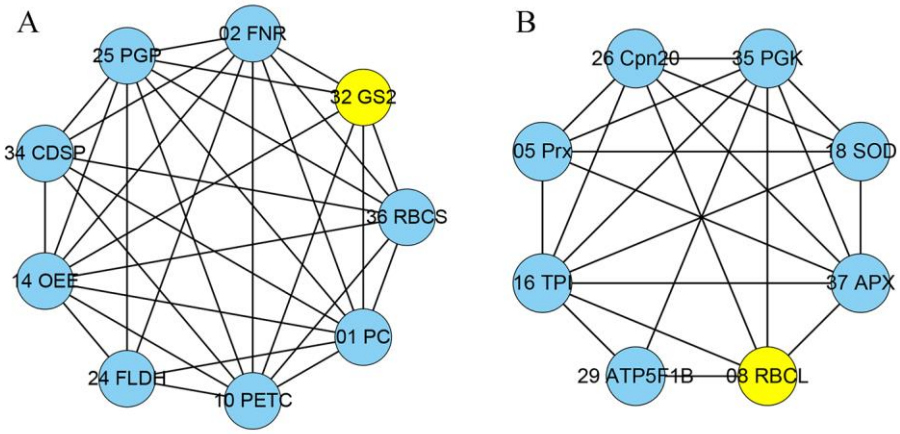

634

635 **Figure 5.** The two modules obtained from the protein-protein interaction network of DEPs. (A) proteins in
636 cluster 1, (B) proteins in cluster 2.

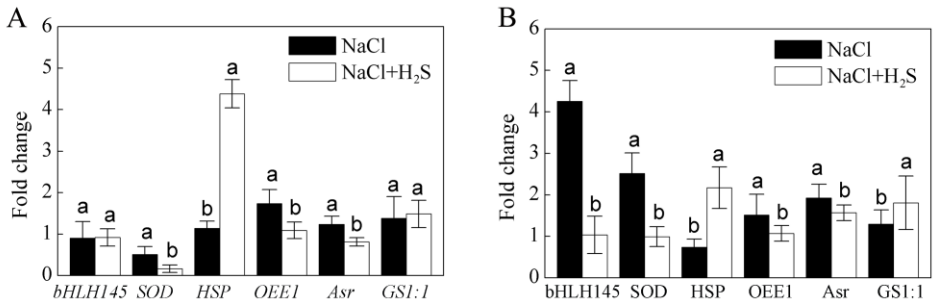

637

638 **Figure 6.** Comparison of expression changes at (A) mRNA and (B) protein levels for the selected six DEPs.
639 They are bHLH 145; superoxide dismutase (SOD); heat-shock protein (HSP); oxygen-evolving enhancer
640 protein 1 (OEE1); abscisic acid stress ripening protein (Asr); glutamine synthetase 1:1 (GS1:1).

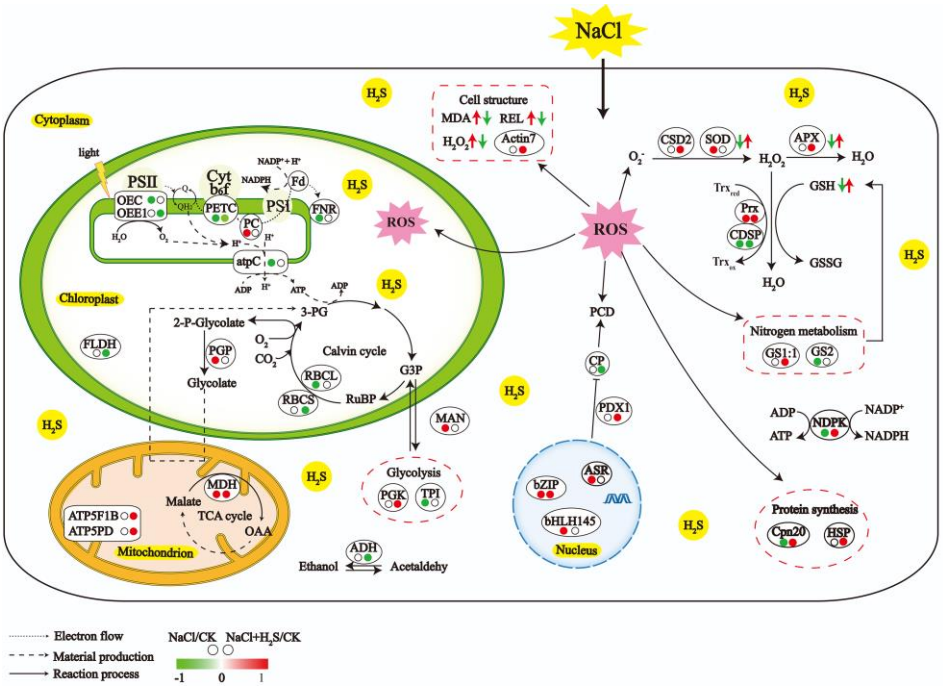

641

642 **Figure 7.** The proposed regulatory networks of H_2S on salt tolerance of *K. obovata* seedling leaves. The
643 left and right dot stand for NaCl and NaCl+H_2S treatment, respectively. The red color of dot indicates the
644 up-regulated change, the green color of dot indicates the down-regulated change, the white color of dot
645 indicates no change in comparison with control. ADH: alcohol dehydrogenase; APX: cytosolic ascorbate
646 peroxidase; Asr: abscisic acid stress ripening protein; atpC: ATP synthase CF1 epsilon subunit; ATP5F1B:
647 ATP synthase beta subunit; ATP5PD: ATP synthase subunit d, mitochondrial; CP: cysteine proteinase; Cpn
648 20: 20 kDa chaperonin family protein; Cpn 60: TCP-1/cpn60 chaperonin family protein; CSD2:
649 copper/zinc superoxide dismutase; CDSP: chloroplastic drought-induced stress protein; FLDH:
650 NAD(P)-binding Rossmann-fold superfamily protein isoform 1; FNR: ferredoxin-NADP reductase; GS2:
651 glutamine synthetase 2; GS1:1: glutamine synthetase 1;1; HSP: heat-shock protein; MAN: Glycosyl
652 hydrolase superfamily protein; MDH: malate dehydrogenase; NDPK: nucleoside diphosphate kinase;
653 OEE1: oxygen-evolving enhancer protein; OEC: O2 evolving complex 33kD family protein; PC:
654 plastocyanin; TPI: triosephosphate isomerase; PCD: programmed cell death; PDX1: pyridoxin biosynthesis;
655 PETC: photosynthetic electron transfer C; PGK: phosphoglycerate kinase; PGP: phosphoglycolate
656 phosphatase; Prx: 2-Cys peroxiredoxin; RBCL: ribulose-1,5-bisphosphate carboxylase large subunit; RBCS:

RuBisCO activase small isoform precursor; SOD: superoxide dismutase; The detailed information for each spot is shown in Table 1.

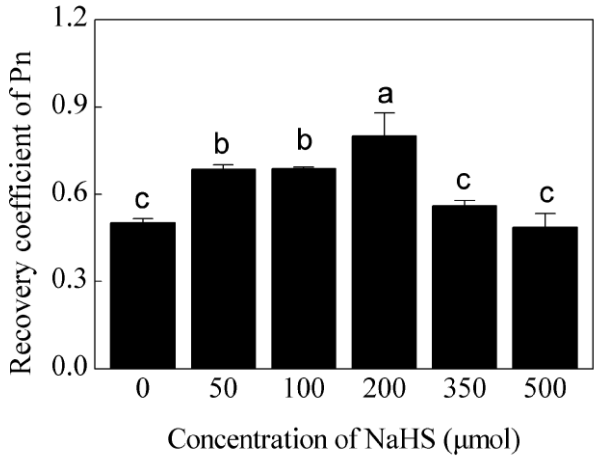

Supplementary Figure S1. Net photosynthetic rate (Pn) recovery coefficient of *K. obovata* seedling leaf under the treatments of series concentration of NaHS. Bars with different letters are significantly different at $P < 0.05$ according to Duncan's multiple range test.

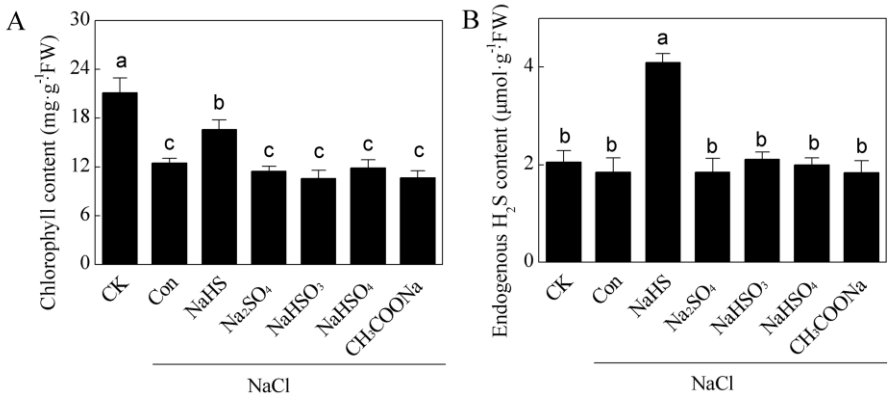

Supplementary Figure S2. H_2S and/or HS^-, but not other compounds derived from NaHS, contribute to (A) chlorophyll content and (B) endogenous H_2S accumulation. *K. obovata* seedlings were treated by 200 μM of NaHS, Na_2SO_4, $NaHSO_3$, $NaHSO_4$, or CH_3COONa, respectively, together with 400 mM NaCl for 7 days. The sample without any above sulfur-containing chemical but with 400 mM NaCl was regarded as the control (Con). CK represents the seedlings without NaCl and any above sulfur-containing chemical. Values

669 are means ± SE of three independent experiments with at least three replicates for each. Bars with different
670 letters are significantly different at $P < 0.05$ according to Duncan's multiple range test.

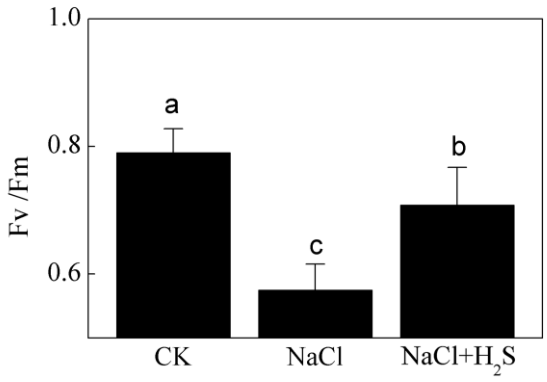

671

672 **Supplementary Figure S3.** Effects of NaHS on chlorophyll fluorescence characteristics of *K. obovata*
673 seedling leaves. CK stands for the control which treated only by 1/4 strength Hoagland's nutrient solution.
674 NaCl stands for 400 mM NaCl treatment. NaCl+H_2S stands for 400 mM NaCl + 200 μM NaHS treatment.
675 Error bars are SE (n=3). The columns labeled with different letters are significantly different at $P < 0.05$.

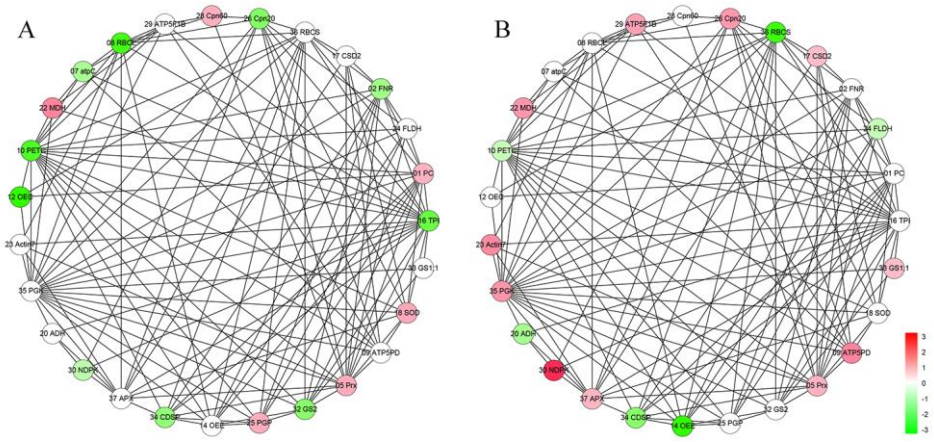

676

677 **Supplementary Figure S4.** Protein–protein interactions (PPIs) network analysis of 27 identified proteins
678 from NaCl and NaHS treated *K. obovata* leaves. The association network was developed by STRING
679 software using the homologous protein accessions from *Arabidopsis thaliana*. (A) the PPI network in NaCl
680 vs CK, (B) the PPI network in NaCl+H_2S vs CK. Nodes in red color represent up-regulated, green color
681 represents down-regulated, white represent no change.

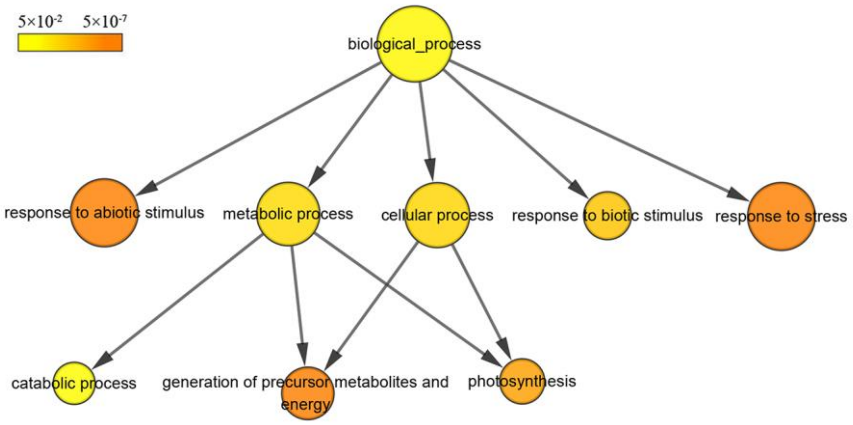

Supplementary Figure S5. Gene ontology analysis of the proteins identified from the leaves of *K. obovata*. Hierarchical directed acyclic graph in the aspect of biological process was performed. The yellow color represents the enriched GO terms.

687 **Table 1.** Identification of differentially expressed proteins with greater than 2.0-fold change in the leaves of *K. obovata* seedlings under salinity and NaHS
688 treatments.

Spot [1]	Accession (gb)[2]	Protein name[3]	Theoretical (Mr/p*I*)[4]	Observed (Mr/p*I*)[5]	Score[6]	MP [7]	Species[8]	Ratio[9]	
								NaCl vs CK	NaCl+H_2S vs CK
Photosynthesis									
1	gi|502131189	PREDICTED: plastocyanin, chloroplastic-like	17.13/5.04	14.05/4.37	118	1	*Cicer arietinum*	2.257	0.841
2	gi|226497434	Ferredoxin-NADP reductase, leaf isozyme	40.98/8.53	37.32/6.74	311	4	*Zea mays*	0.287	0.686
8	gi|363981020	Ribulose-1,5-bisphosphate carboxylase/oxygenase large subunit, partial (chloroplast)	50.67/5.87	19.87/5.19	116	7	*Cercidiphyllum japonicum*	0.086	0.736
10	gi|508707371	Photosynthetic electron transfer C	24.67/8.15	19.14/4.79	103	5	*Theobroma cacao*	0.100	0.483
12	gi|222853091	O_2 evolving complex 33kD family protein	35.41/5.85	36.80/5.22	405	4	*Populus trichocarpa*	0.067	0.518
14	gi|527190719	Oxygen-evolving enhancer protein 1, chloroplastic	34.80/6.48	34.78/5.47	493	8	*Genlisea aurea*	1.213	0.068
36	gi|62733297	RuBisCO activase small isoform precursor	52.39/5.59	42.29/5.03	276	7	*Oryza sativa* Japonica Group	0.741	0.079
Carbohydrate and energy metabolism									
6	gi|508785499	Glycosyl hydrolase superfamily protein, putative	37.45/8.39	34.33/4.66	68	1	*Theobroma cacao*	2.072	1.279
7	gi|336041766	ATP synthase CF1 epsilon subunit	13.69/5.43	14.89/5.03	97	2	*Justicia americana*	0.323	0.528
9	gi|460411739	PREDICTED: ATP synthase subunit d, mitochondrial-like	19.78/5.33	18.95/5.04	119	4	*Solanum lycopersicum*	0.704	3.630
16	gi|508786769	Triosephosphate isomerase	27.50/5.54	23.96/6.35	164	7	*Theobroma cacao*	0.142	0.605
20	gi|223535342	Alcohol dehydrogenase, putative	41.61/8.61	37.23/5.88	513	6	*Ricinus communis*	0.643	0.311
22	gi|226503019	Malate dehydrogenase, cytoplasmic	35.85/5.76	40.48/6.78	250	7	*Zea mays*	3.659	2.997
24	gi|508715598	NAD(P)-binding Rossmann-fold	36.50/9.29	28.24/5.53	268	4	*Theobroma cacao*	0.663	0.469

		superfamily protein isoform 1							
25	gi|502105712	Phosphoglycolate phosphatase	40.78/6.89	37.32/6.74	226	10	*Cicer arietinum*	2.400	1.927
29	gi|335059237	ATP synthase beta subunit	52.29/5.09	57.59/4.97	453	11	*Clerodendrum trichotomum*	1.591	2.706
30	gi|475549973	Nucleoside diphosphate kinase 1	17.03/6.85	16.16/6.40	107	5	*Aegilops tauschii*	0.419	9.366
35	gi|223547261	Phosphoglycerate kinase, putative	50.11/8.74	51.05/5.99	294	6	*Ricinus communis*	1.115	3.040
Amino acid and protein metabolism									
4	gi|355492134	Cysteine proteinase	54.16/5.27	40.03 /4.48	93	4	*Medicago truncatula*	1.512	0.162
19	gi|223544592	Heat-shock protein, putative	17.81/5.93	16.81/5.69	129	6	*Ricinus communis*	0.734	2.172
26	gi|550336292	20 kDa chaperonin family protein	26.89/8.75	23.19/5.62	245	5	*Populus trichocarpa*	0.196	2.934
28	gi|508779629	TCP-1/cpn60 chaperonin family protein	65.05/5.57	56.09/5.27	714	15	*Theobroma cacao*	2.301	1.562
32	gi|508713595	Glutamine synthetase 2	61.64/8.38	44.25/5.98	63	3	*Theobroma cacao*	0.208	1.068
33	gi|332006826	Glutamine synthetase 1;1	39.32/5.28	40.86/5.71	241	7	*Arabidopsis thaliana*	1.294	1.807
Hormone biosynthesis and transcription factor									
13	gi|332008500	Transcription factor bHLH145	35.26/5.08	40.10/5.52	64	11	*Arabidopsis thaliana*	4.254	1.032
21	gi|508712975	Mitochondrial transcription termination factor family protein, putative isoform 1	51.01/9.32	44.71/6.38	56	11	*Theobroma cacao*	0.252	0.393
27	gi|355514936	BZIP transcription factor	24.12/8.65	23.37/5.88	60	9	*Medicago truncatula*	2.478	3.198
31	gi|355481146	Abscisic acid stress ripening protein	27.33/5.15	39.71/5.9	207	2	*Medicago truncatula*	2.024	1.567
Stress response proteins									
5	gi|502112102	PREDICTED: 2-Cys peroxiredoxin BAS1-like, chloroplastic-like isoform X2	29.14/6.12	21.46/4.96	361	6	*Cucumis sativus*	2.446	2.257
11	gi|222867611	Pyridoxin biosynthesis PDX1-like protein 3	33.31/6.55	15.98/5.29	60	8	*Populus trichocarpa*	0.886	2.230
17	gi|409900374	Copper/zinc superoxide dismutase	23.29/6.12	19.07/5.74	393	4	*Musa acuminata*	1.184	2.006

		CSD2A-1							
18	gi|414866828	Superoxide dismutase 4	15.65/5.10	15.02/5.80	77	3	*Zea mays*	2.510	0.988
23	gi|508776520	Actin 7 isoform 1	41.80/5.31	43.65/5.52	342	9	*Theobroma cacao*	0.827	3.400
34	gi|508723241	Chloroplastic drought-induced stress protein of 32 kD	40.91/7.66	27.45/5.77	213	6	*Theobroma cacao*	0.237	0.210
37	gi|498923199	Cytosolic ascorbate peroxidase	27.09/5.52	32.52/6.66	234	3	*Arachis hypogaea*	0.734	2.172
Unknown protein									
3	gi|548848586	Hypothetical protein AMTR_s00157p00064680	54.99/6.91	28.30/4.86	68	1	*Amborella trichopoda*	0.120	0.759
15	gi|462410037	Hypothetical protein PRUPE_ppa019045mg	25.73/5.65	29.45/6.01	150	5	*Prunus persica*	0.488	0.669

[1]The spot number corresponding to the number listed in the table.

[2]Database accession numbers (gb) according to NCBInr.

[3]The names of proteins were identified by LC-MALDI-TOF/TOF.

[4]Theoretical mass (kDa) and p*I* of identified proteins. Theoretical values were retrieved from the NCBInr database.

[5]Experimental mass (kDa) and p*I* of identified proteins. Experimental values were calculated by using PDquest software and standard molecular mass markers.

[6] Number of matched peptide fragments.

[7]The Mascot searched score against the database NCBInr.

[8]The species which has the high homology of the identified protein.

[9]Ratio between the different treatments. NaCl vs CK means 400 mM NaCl vs control; NaCl+H_2S vs CK means 400 mM NaCl + 200 μM NaHS vs control

Supplementary Table S1. Sequences of forward and reverse primers used in qRT-PCR for gene expression analysis in *K. obovata* leaves.

Spot number	Gene name	Annealing temperature	Forward primer sequence (5' to 3')
18	*bHLH145*	59°C	F: GATGTTGCATGTGTTGGAGAAG
			R: GAGAGAGATGTGTGGACTGAAAG
24	*SOD*	59°C	F: GCTTTGACCCAGGAAGATGA
			R: CATTTGTTGTGTCGCCATACTC
25	*HSP*	59°C	F: GCAGGAGGAGAAGAACGATAAG
			R: CCATGCTAGCTTTGACCTGATA
46	*OEE1*	59°C	F: AGGTGGCCTTGATTCTCAAATA
			R: CAGCATGTATAGGCTCGGAAA
48	*Asr*	59°C	F: ATGACAGCAAGCCAAAGAGA
			R: CTCCTACAGAGCGAGTGATAGA
50	*GS1:1*	59°C	F: GAGACAACCATCCTCTGGAAAC
			R: GTGGTGGAACTTAGGCAAACTA
	actin	59°C	F: AGCATCAGGCATCCATGAGAC
			R: TGCTGAGAGATGCCAGAATG

Supplementary Table S2. Co-relations among different physiological indices in *K. obovata* leaves.

	DW	Chl	Ci	Pn	Gs	Tr
DW		0.379	0.042	0.500*	0.352	0.804**
Chl			-0.655*	0.895*	0.825**	0.406
Ci				-0.645**	-0.655**	-0.133
Pn					0.839**	0.695**
GS						0.469*

* Correlation is significant at the 0.05 level (2-tailed). ** Correlation is significant at the 0.01 level (2-tailed)

Supplementary Table S3. The modules of the protein-protein interaction networks and nodes biological process (GO) analysis

Module name	Nodes	Edges	Cluster scores	Term ID	Term description	FDR	Matching nodes
A	9	32	8	GO: 0050896	response to stimulus	3.7×10^{-4}	CDSP, FLDH, FNR, GS2, OEE, PC, PETC, RBCS
B	8	22	6.286	GO: 0009628	response to abiotic stimulus	8.6×10^{-5}	APX, Cpn20, TPI, PGK, Prx, SOD

710 **Supplementary Table S4.** The detail information of the peptide sequence, expected and observed m/z
711 values, sequence coverage for the different expressed proteins identified by MALDI-TOF/TOF MS in the
712 leaves of *K. obovata*. under the salinity and NaHS treatments.

Spot	Sequence[1]	Theoretical (Mr)[2]	Observed (Mr)[3]
Photosynthesis			
1	NNAGFPHNVVFDEDEIPS GVDATK	17128.7	14050
2	LDFAVSR	40976.5	37320
	MYIQTR		
	DPNATVIMLATGTGIAPF R		
	ITGDDAPGETWHMVFST EGEIPYR		
8	EGNEIIR	50671.4	19870
	DDFIEKDR		
	EGNEIIREASK		
	TYYTPDYETK		
	LEDLRIPAAYAK		
	TFQGPPHGIQVER		
	GHYLNATAGTCEEMIK		
10	FYWAPTR	30594.1	58180
	EGPPEFEQPK		
	SFQCELVFAK		
	MCCLFINDLDAGAGR		
	LVNSREGPPEFEQPK		
	IVDSFPGQSIDFFGALR		
	MCCLFINDLDAGAGR		
12	VPFLFTIK	35412	36800
	RLTYEEIQSK		
	GGSTGYDNAVALPAGGR		
	DGIDYAAVTVQLPGGER		
14	STASVPIR	34802.9	34780
	VPFLFTIK		
	DGIDYAAVTVQLPGGER		
	FVEKDGIDYAAVTVQLPG GER		
36	FYWAPTR	52394	42290
	VPLILGIWGGK		
	EGPPEFEQPK		
	SFQCELVFAK		
	MCCLFINDLDAGAGR		
	IVDSFPGQSIDFFGALR		
	QVTSAVNYHGKSSNINR		
Carbohydrate and energy metabolism			
6	RPGKPIETYLFAMFDENQK	37447.3	34330
7	QIIEANLALR	13694.4	14890
	LNGEWLTMALMGGFAR		
9	KFDDEIR	19781.1	18950
	TIDWDGMAK		

	FDDEIRNDYWGY		
	FSQEPEPINWEYYR		
16	FFVGGNWK	27497.2	23960
	KFFVGGNWK		
	CNGTTEEVKK		
	ALLNESNEFVGDK		
	SDFHVAAQNCWVR		
	ELAAQPDVDGFLVGGASLKPEFIDIIK		
	ELAAQPDVDGFLVGGAS LKPEFIDIIKAATVK		
20	AWVYGEYGGVDVLK	41607.1	37230
	FDVVYDAIGQCDR		
	QFGSLAEYTAVEEK		
	EGGSVVALTGAVTPPGFR		
	GPFPFSQVAEAFSYIETNR		
	ENFEDLPEKFDVVYDAIGQCDR		
22	MAKEPMR	35846.3	40480
	ALGQISER		
	VLVVANPANTNALILK		
	FSSALSAASSACDHIR		
	KFSSALSAASSACDHIR		
	VLVTGAAGQIGYALVPMIAR		
	NVIIWGNHSSTQYPDVNHATVK		
24	MKPGFDPTK	36499	28240
	SDQFVTRGLVR		
	AEQYLADSGVPYTIIR		
	KAEQYLADSGVPYTIIR		
25	ISDFLSLK	40783.6	37320
	SQICMVGDR		
	IQYGTLCIR		
	VYVIGEDGILK		
	ISDFLSLKAAAV		
	NPLLSSNSAFLK		
	LVFVTNNSTKSR		
	ENPGCLFIATNR		
	GDSLIEGVPETLDMLR		
	EPLVVGKPSTFMMDYLANEFGISK		
29	MPNIYNALVVK	52293.2	57590
	TVAMSATDGLMR		
	AHGGVSVFGGVGER		
	FVQAGSEVSALLGR		
	VGLTALTMAEYFR		
	VALVYGQMNEPPGAR		
	DVNEQDVLLFIDNIFR		
	GMEVIDTGAPLSVPVGGATLGR		
	ELQDIIAILGLDELSEEDR		
	MPSAVGYQPTLSTEMGSLQER		
	IFNVLGEPVDNLGPVDTRTTFPIHR		
30	GLKLQNVEK	17034.8	16160
	SSQHNWIYEA		

	NVIHGSDSVESAR		
	EIALWFPEGIAEWR		
	ASEQTFIMIKPDGVQR		
35	NEPEFAK	50114	51050
	FSLAPLVPR		
	ASRAVVSMAK		
	VILSSHLGRPK		
	LVASLPEGGVLLLENVR		
	LASLADLYVNDAFGTAHR		
Amino acid and protein metabolism			
4	NLAASVAGK	53517.9	40030
	DNPFGVKAMK		
	EVKNIYEEWR		
	AVANQPISVAIEAGGR		
	TPAKLHWPFGDQNK		
19	DAKAMASTPADVK	17808.1	16810
	VQVEDDNVLLISGER		
26	YAGNDFK	26898.4	23190
	IKIAEEK		
	DLKPLNDR		
	TAGGLLLTEATK		
	DLKPLNDRVLIK		
28	KLQTGVNK	65045.9	56090
	AEKEVLGQAAK		
	LADLVGVTLGPK		
	IAALKAPGFGER		
	VVAAGANPVQITK		
	GYISPYFVTDSEK		
	AAVEEGIVVGGGCTLLR		
	SQYLDDIAILTGGTVIR		
	LSGGVAVIQVGAQTETELK		
	SAENNLYVVEGMQFDR		
	KSQYLDDIAILTGGTVIR		
	LSGGVAVIQVGAQTETELKEK		
32	VGRDTEK	61638.1	44250
	AMVHRQMGQEVGNR		
	IIAEYIWIGGSGIDLR		
33	VGRDTEK	39318.5	40860
	EHIAAYGEGNER		
	HKEHIAAYGEGNER		
	IIAEYIWVGGSGMDMR		
	RPASNMDPYIVTSMIAETTILWNP		
	LTGHHETADINTFLWGVANRGASIR		
Hormone biosynthesis and transcription factor			
13	SLKMEAK	35262.1	40100
	QDLNLVSK		
	AEEQCSQK		
	QHACPDMK		
	EELQRSNK		

	AEEQCSQKR		
	ILETSNESMR		
	KILETSNESMR		
	QHACPDMKEELQR		
	SFETLKQHACPDMK		
	RFLVFDQSGDQTTLLLASDIR		
21	WQIGISK	51008.1	44710
	MAVTSLTK		
	ILWKEPR		
	IEFLVNRMK		
	VLGMALGEMSR		
	FQIDPDGFLK		
	AVTSLTKATTLK		
	VEFFEGIGIPR		
	LVLYEIEEIEK		
	VFYLFPEVLGLDIGNR		
27	NMENAVADLTK	24115.5	23370
	AMAYHSGIGISK		
	LNSVLENQIFT		
	MAMAYHSGIGISK		
	LANEVKHLSSNR		
	LSDLIGDLQALVK		
	VLFIAVTGYTGTVLLK		
	VLFIAVTGYTGTVLLKNGK		
	VQDTVTTIHDDLSVVQHTVKMLDGR		
31	TTTGGGYGGGYGDSDTK	27332.2	39710
	HKIEEEVAAVAAVGSGGFAFHEHHEK		
Stress response proteins			
5	SVDETKR	29144.1	21460
	SYGVLIPDQGIALR		
	EGVIQHSTINNLAIGR		
	SGGLGDLNYPLVSDVTKSISK		
	GLFIIDKEGVIQHSTINNLAIGR		
	TLQALQYVQENPDEVCPAGWKPGEK		
11	HVRSVMGDIR	33308.2	15980
	QAVTIPVMAKAR		
	VPADIRAQGGVAR		
	KIAAPYDLVMQTK		
	AQGGVARMSDPQLIK		
	AGTGVVAVYGNGAITETK		
	MAGTGVVAVYGNGAITETK		
	VGLAQMLRGGVIMDVVTPEQAR		
17	SAPLGQPFR	23291.9	19070
	GGHELSLTTGNAGGR		
	AFVVHELEDDLGK		
	AFVVHELEDDLGKGGHELSLTTGNAGGR		
18	EHGAPEDENR	15645.6	15020
	AVVVHADPDDLGK		
	FCVFVCVECGGAFPLF		

23	AGFAGDDAPR	41801.1	43650
	GYSFTTTAER		
	AVFPSIVGRPR		
	AEYDESGPSIVHR		
	IWHHTFYNELR		
	AEYDESGPSIVHRK		
	SYELPDGQVITIGAER		
	VAPEEHPVLLTEAPLNPK		
	DLYGNIVLSGGSTMFPGIADR		
34	LEASKTR	40911.9	27450
	GELIGEILR		
	VPHFSFYK		
	HCGPCVKVYPTVIK		
	DMDVIEVPTFLFIR		
	TCNDVEFILVMGDESEK		
37	EDKPEPPPEGR	27090.8	32520
	ELLSGEKEGLLQLPSDK		
	YAADEDAFFADYAEAHLK		
Unknown protein			
3	SMEVVSGFR	54990.9	28300
15	GEEQEEAK	25734.2	29450
	FWVDYIDK		
	APLLPSDPYQR		
	DKAPLLPSDPYQR		
	CMQKESVAQSLADPK		

[1]The peptide sequence. C represent modification of carbamidomethyl, O represent modification of oxidation.

[2]The theoretical m/z, mass over charge ratio of the parent ion.

[3]The experimental m/z, mass over charge ratio of the parent ion.